X-ray reflectometry characterization of porous silicon films prepared by a glancing-angle deposition method

S. Asgharizadeh and M. Sutton
Department of Physics and Centre for the Physics of Materials, McGill University, 3600 University Street, Montreal, Quebec, Canada H3A 2T8

K. Robbie and T. Brown
Department of Physics, Queen's University, Kingston, Ontario, Canada K7L 3N6
(Received 20 May 2008; published 4 March 2009)

The competitive growth process of ballistic deposition is studied experimentally using x-ray reflectivity characterization of silicon thin films deposited with various vapor incidence angles. Linear profiles of film density with thickness are shown to reproduce the observed reflectivity spectra. A porosity of about 10% was observed in the first few atomic layers atop the substrate, with porosity decreasing with film thickness to near zero for vapor incidence between normal and 60°, and porosity increasing to 50% and above for vapor incidence angles above 70°—the regime of glancing-angle deposition. Our results support the model of glancing deposition as sequential atomic ballistic deposition, where the observed sign change in the slope of the density profile is understood to correspond to the geometric condition where the roughening caused by self-shadowing overtakes the smoothing effects of atomic surface diffusion. From the electron-density profiles derived from x-ray reflectivity measurements, we calculate the average porosity and using data on optical indices of refraction we estimate the amount of silicon oxide.

DOI: 10.1103/PhysRevB.79.125405 PACS number(s): 61.05.cm, 68.55.−a, 81.15.−z

I. INTRODUCTION

Silicon that has been processed in some manner to include nanometer-scale pores is an interesting material for scientific study and potential technological application. While several methods exist for creating porous silicon,[1–3] the topic of our study is silicon thin films deposited from atomic vapor in vacuum.[4] Controlling growth conditions such as temperature and deposition rate are known to affect the bonding process that each incoming atom experiences upon arrival at the substrate, and controlling the geometry of the arriving vapor affects the probability that an incoming atom will arrive at a particular location on the growing film surface. A unique growth regime was discovered to exist when vapor arrives at a glancing incidence onto a substrate (vapor arriving at an angle greater than approximately 70° from the substrate normal) characterized by extremely porous film structures composed of columns oriented toward the vapor source. This growth regime, called glancing-angle deposition (GLAD), exploits the sensitive dependence of atomic-scale structure on growth geometry—allowing macroscopic changes to the deposition equipment to affect atomic surface growth and creating another class of nanoengineered materials. Demonstrated novel materials include circular polarizers,[5] graded antireflection (AR) coatings, and several forms of photonic crystals.[6]

The columnar structure of thin solid films has been widely studied, with the structure understood to be a consequence of atomic self-shadowing (where previously deposited film material geometrically blocks the path of subsequently arriving atoms, preventing vapor impingement into shadowed regions). When surface diffusion is limited (such as for deposition onto a cold substrate) atoms bond to the growing film surface very near to where they ballistically arrive, and the resulting film morphology is similar to the branching fractal structures seen in diffusion-limited aggregation (DLA).[7–10] A schematic model of the growth process is shown in Fig. 1(a) where the vapor is shown to arrive from the right side at 80° from the substrate normal, creating strong shadowing and inducing a highly porous film structure composed of columns growing at an angle between the vapor arrival vector and the substrate normal. As the vapor incidence angle is brought from normal to glancing, the effects of shadowing become more significant and the film porosity continually increases. The shadowing effect combined with the stochastic arrival of the atomic vapor leads to continuous competition between columns, and columns losing out continuously in time. These "extinguished" columns become unable to capture incoming vapor due to shadows cast by neighboring columns, and they therefore stop growing.[11] At the other extreme of growth conditions (such as for deposition onto a hot substrate), where atoms are able to diffuse significant distances across the growing surface, the diffusing atoms tend to fill the regions which were shadowed by previous growth, resulting in a dense bulklike morphology. This competition between self-shadowing and surface diffusion defines the evolution of the growing film surface and ultimately the resulting film morphology.[12,13]

Despite extensive study of thin films fabricated with off-normal vapor incidence, more work is needed to understand the relationship between growth conditions and film morphology. While scanning electron microscopy (SEM) has revealed useful insights into film structure,[14,15] accurate measurements of porosity are not possible due to the limited resolution of the SEM (approximately 10 nm) and its inability to probe the internal structure of three-dimensional film morphologies. Film porosities were measured gravimetrically for several materials by weighing a piece of the film

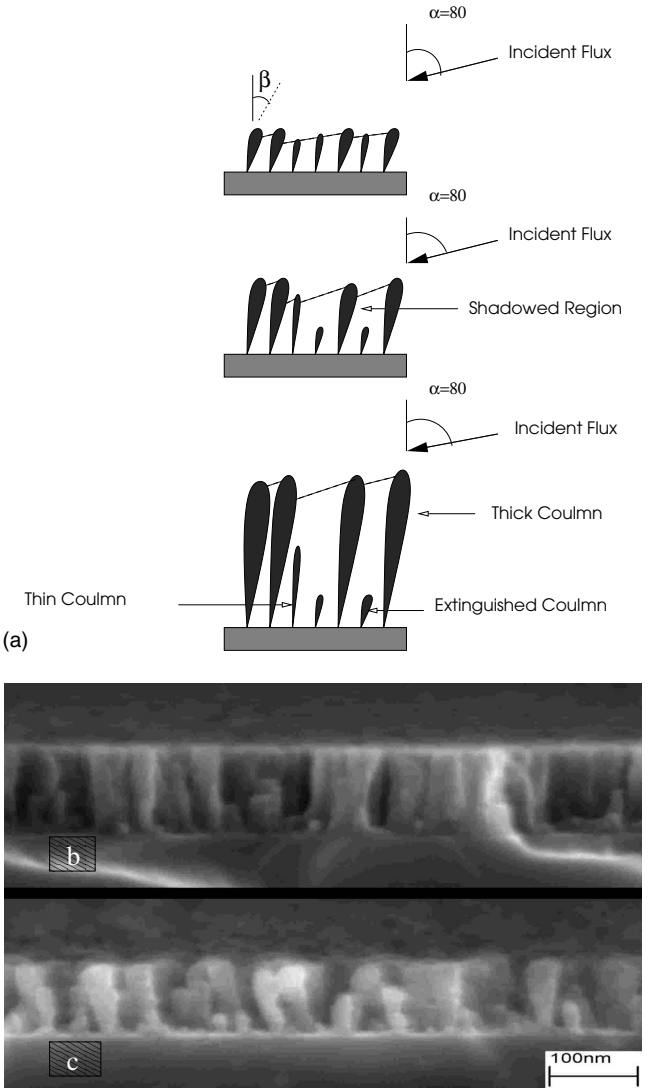

FIG. 1. (a) Due to shadowing some columns disappear in the regions close to the substrate and some thinner columns extend more. α and γ are flux angle and average column orientation, respectively. A SEM picture of the fracture cross sections of two 100-nm-thick films deposited with vapor incident at (b) 80° and (c) 85°.

and substrate then etching away the film and reweighing the bare substrate.[15] This method for measuring porosity is not highly accurate and yields only an average porosity for the film, not a porosity profile as a function of film thickness.

Kaminska *et al.*[16] measured film thicknesses and optical indices of refraction with a combination of variable-angle spectroscopic ellipsometry (VASE) and SEM. The SEM analysis was performed solely on plan-view images and therefore neglected porosity not visible from this top view. In this work Kaminska concludes that for silicon films, prepared with vapor arriving at 87° from normal, the porosity increases with the sample thickness.

X-ray reflectivity (XRR) is a nondestructive tool well suited to investigate thin layers. Unlike most other techniques, it reveals the electron density versus depth of the sample under study, as well as thickness and surface roughness to a subangstrom resolution. Regression analysis is used to fit a theoretical electron-density profile (EDP) (the density of electrons in a film as a function of distance from the substrate) to measured XRR spectra for each film; the resulting EDP is used to calculate porosity and refractive index, revealing physical properties of the films as well as providing insight into the atomistic dynamics of the film growth process.

The aim of this paper is to use XRR to extract EDPs of thin films made by GLAD technique. The electron density was well modeled by a linear density profile, with electron density found to increase with thickness (porosity decreasing) for nonglancing films, and decrease with thickness (porosity increasing) for films deposited with vapor arriving at an angle of 70° or larger from the substrate normal. We observe directly the transition from surface-diffusion-dominated to shadowing-dominated growth. Effective optical index of refraction is calculated from measured porosity profiles.

II. THEORY

The complex index of refraction for x rays is given by

$$n = 1 - \delta - i\beta. \tag{1}$$

The real and imaginary parts denote the dispersion and absorption of x rays in a dielectric medium, respectively.[17] In a homogeneous medium and far away from absorption edges, δ and β are

$$\delta = \frac{\lambda^2}{2\pi} r_e \rho \tag{2}$$

and

$$\beta = \frac{\lambda}{4\pi} \mu, \tag{3}$$

where r_e (2.814×10^{-5} Å) and ρ are the electron radius and electron density ($e/\text{Å}^3$), respectively. The linear absorption coefficient is μ and λ is the incident wavelength. The critical angle for total reflection of x rays from a layer is proportional to the mean density value of the layer and is given by[18]

$$\theta_c \approx \sqrt{2\delta} = \lambda \sqrt{(r_e \rho / \pi)}. \tag{4}$$

For incident angles $\theta \leq \theta_c$ total external reflection occurs and x rays do not penetrate very far into the medium. Thus all incoming radiation is reflected (with small losses due to absorption). For $\theta > \theta_c$, the intensity of specular reflectivity for an ideal surface with no roughness falls off as $\frac{1}{(2\theta)^4}$,[19] whereas for a rough surface it falls off faster as a result of multiplication of the reflectivity by a Debye-Waller-type factor.[20] The periodicity of peaks in the reflectivity curve is determined by the thickness of the layer with the spacing between maxima in reciprocal space given by $\delta q_z = 2\pi n/d$ for a layer with index of refraction n and thickness d.

III. EXPERIMENT

A series of silicon thin films was prepared using the glancing-angle deposition technique.[4,5] Silicon was vapor-

ized with an electron-beam evaporator and allowed to condense onto glass or silicon substrates held by a motor-controlled manipulator. The manipulator oriented each substrate at a fixed deposition angle relative to the incoming vapor then rapidly rotated during film growth (so chosen to maintain rotational symmetry in the resulting film structure). This results in a vapor distribution slightly different from that shown in the schematic of Fig. 1(a) as the vapor does not arrive from only one side, but in fact arrives equally from all azimuthal angles, creating a vertical, instead of slanted, columnar film [Figs. 1(b) and 1(c)]. The deposition rate was set to 0.5 nm/s, and the substrate was chosen to rotate once for each 1 nm of deposited film—so the rotation period was 2 s and the rate was 0.5 Hz or 30 rpm. The substrate temperature was not controlled during film growth but is believed to have been approximately 50 °C. Given these growth conditions the silicon films are expected to be columnar and amorphous, although their crystallinity was not characterized in this study. Once each film was deposited, it was brought out of the vacuum chamber to atmosphere and stored in air. Oxidation of these silicon films by atmospheric oxygen is the subject of another ongoing study, but we do know that the samples used in this study underwent partial oxidation over several months to yield a stable structure of silicon in the column cores encased in a layer of silica.[16]

A high-resolution diffractometer, with a copper x-ray tube, is used to collect the data. Two germanium crystals act as analyzer and monochromator with a 3×10^{-5} rad width for their (111) reflection. To obtain specular reflectivity, θ-rocking curves around $\theta=\frac{2\theta}{2}(\omega=0)$ are done. This allows for the true specular reflectivity to be obtained by subtracting the diffuse scattering at each 2θ point.[21]

Considering the length of the sample parallel to the beam (20–25 mm) and the width of the beam in the horizontal direction (0.8 mm) a foot print correction is imposed.[17,18,21] Equivalently, one can divide the experimental data by $\sin(\theta)$ in order to take into account the variation in the area of the x-ray beam intersected by the sample.

IV. RESULTS AND DISCUSSION

A. X-ray reflectivity measurements

We measured the specular x-ray reflectivity for a set of porous silicon films with various thicknesses deposited with vapor incidence angles between 0° (vapor arrives along surface normal) and 80° (vapor arrives at a glancing angle), $0°\leq\alpha\leq80°$. The measured reflectivity spectra were compared with calculated theoretical spectra assuming linear electron-density profiles, yielding the film thickness and the electron-density profile.

From the critical angle, a coarse estimate of the average density of the top layers of a film [Eq. (4)] can be calculated. Porous structures allow x rays to scatter from deeper in the film. Figure 2 depicts three reflectivity curves of a thick dense silicon substrate as well as two porous GLAD samples with 60° and 80° deposition angles versus the momentum transferred to the film along the direction perpendicular to the surface ($q_z=\frac{4\pi}{\lambda}\sin\theta$). The vertical dashed line marks the

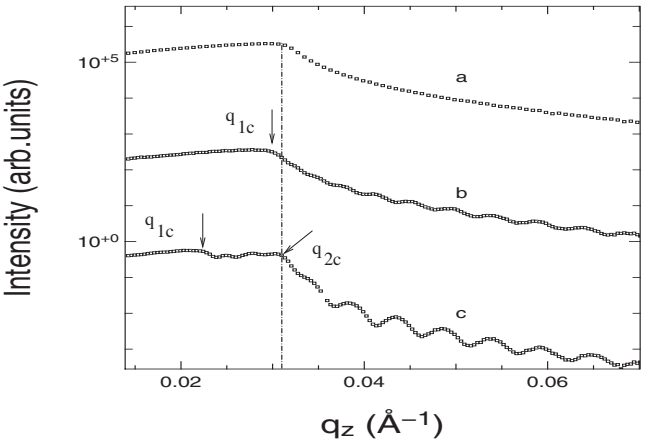

FIG. 2. Reflectivity curves for (a) dense nonpolished Si layer, (b) 60° sample, and (c) 80° sample on silicon substrates. The dashed line specifies the critical angle of dense Si. The curves have been scaled by (a) 10^0, (b) 10^{-2}, and (c) 10^{-4} for clarity.

critical angle for dense Si. These three reflectivity curves reveal the following:

(i) For an uncoated silicon substrate there is total reflection of the x rays for $q_z\leq0.031$ Å^{-1} and only evanescent waves propagate in the top layers of the sample. Equation (4) gives 0.7 $e/$Å^3 mean electron density ($\theta_c=0.22°$). Thickness fringes are not observed due to the large thickness of the substrate. The reflectivity curve, as a result of surface roughness and Fresnel reflectivity, falls off with q_z.

(ii) For the 60° sample of nominal thickness 1000 Å, the critical angle is shifted to a lower value ($q_z=0.029$ Å^{-1}). This is evidence of formation of porous layers in the sample. Thickness fringes, as a result of interference of the reflected wave from substrate and porous layer, are observed and show that the densities of the substrate and film are different. The amplitude of these fringes is a more sensitive measure of the change in electron density.

(iii) For the 80° sample also of nominal thickness 1000 Å, two critical angles ($q_{1c}=0.02$ Å^{-1} and $q_{2c}=0.03$ Å^{-1}) associated with the porous film and the substrate can be seen. Equation (4) gives 0.36 and 0.7 $e/$Å^3 corresponding electron densities. Between these two critical angles, the reflected intensity is close to the incident intensity. In this region, x rays penetrate into the porous layer then are totally reflected by the substrate, resulting in waveguide fringes. According to the geometrical optics, the maxima of oscillations in a film with thickness d are described by a formula as

$$\theta_m^2=\theta_c^2+m^2\left(\frac{\lambda}{2d}\right)^2, \tag{5}$$

where $m=0,1,2,\ldots$ and θ_c is the first critical angle in the reflectivity curve. Two maxima, at $q_z=0.024$ Å^{-1} and $q_z=0.027$ Å^{-1}, respectively, can be seen. This indicates a remarkable amount of porosity for this sample. These two critical angles associated with top layers of the film and silicon substrate can be used in Eq. (5) to estimate the thickness of the film to be ≈1000 Å. In the reflectivity curve, above

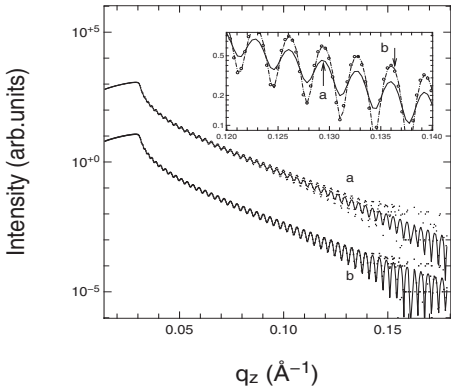

FIG. 3. Calculated and experimental reflectivity from 0° GLAD sample on silicon substrate (a) with a one-layer density calculated by critical angle and (b) with a linear density profile. Inset shows the difference between the two model reflectivities. The one-layer model fails to fit the data for higher q_z's. Plot (b) is shifted on intensity axis by a factor of 10 for clarity. The same data points are used in both curves.

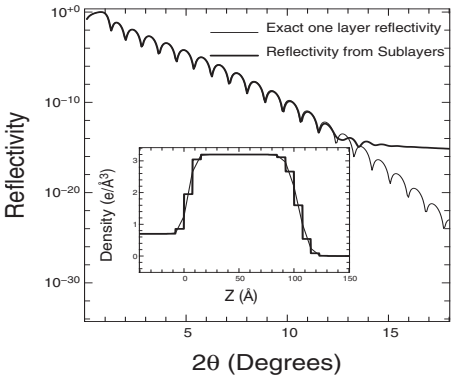

FIG. 4. Calculated reflectivity using a model of 100 sublayers showing agreement with the exact reflectivity curve up to $2\theta=11°$. Shown in inset is a continuous density profile of a layer with 3.2 $e/\text{Å}^3$ density divided up into nine sublayers to emphasize discreteness. Reflectivity was calculated for 100 sublayers which is also plotted in the inset and is indistinguishable from the continuous profile.

critical angle of silicon, relatively large amplitude oscillations can be seen showing a larger difference in densities between the substrate and film.

Our experiments for samples fabricated with smaller deposition angles show less porosity. Nevertheless, XRR of all GLAD samples in the range of deposition angle $0° \leq \alpha \leq 80°$ reveals that all samples have some degree of porosity, which increases with increased deposition angle.

B. Modeling

We fit our experimental data using a model from Vidal and Vincent[22] which calculates the reflectivity from a stack of thin films using a matrix for each layer in the stack. Figure 3(a) illustrates a fit to the 0° sample (nominal thickness 2000 Å) on a silicon substrate modeled as a single constant-density layer with a roughness at the two interfaces, top and bottom. The low amplitude oscillations show that the density of the thin film is slightly different from that of the Si substrate; however, the model clearly does not fit the data well. In particular, it fails to reproduce the observed feature of increasing oscillation amplitude with q_z. When a linear depth-dependent density $\rho(z)$ is used, the fit is much better (curve b in Fig. 3).

There does not seem to be a simple model to calculate the reflectivity for an arbitrary density profile $\rho(z)$. We use a simple discretized model consisting of layers of constant density for which the Vidal and Vincent matrix model can be used. We divide the layer into N layers each with a density matching the appropriate value of $\rho(z)$ as demonstrated in the inset of Fig. 4. Each of the N sublayers is described by a thickness, roughness, electron density, and linear absorption parameters. In Fig. 4 we compare the reflectivity from this N-layer model to the exact calculation for a single layer with erfc(z) interfaces. The figure shows the reflectivity of 100 Å thick layer of $\rho=3.2$ $e/\text{Å}^3$ on a silicon substrate. The 100-layer approximation and the exact calculation are in excellent agreement below $2\theta=11°$. The calculation is extended to $2\theta=18°$ to show that the approximation breaks down for large wave vectors where the discreteness of the layers becomes a significant effect.

For porous films, we model the electron density by a linear density

$$\rho(z_N) = \rho_{\text{bottom}} + \left(\frac{\rho_{\text{top}} - \rho_{\text{bottom}}}{d}\right) z_N, \tag{6}$$

where $\rho(z_N)$, ρ_{bottom}, and ρ_{top} are densities at depth z_N, the bottom, and the top of the film and d is the thickness of the layer. The linear absorption of each sublayer at depth z_N is determined by the fraction $\frac{\rho(z_N)}{\rho_{\text{Si}}}$ times the linear absorption coefficient of silicon. Furthermore, we use a complementary error function to describe the density profile at the substrate-film and film-vacuum interfaces.[23] So the EDP used to fit the data is

$$\rho(z) = \frac{1}{2}\sum_{i=1}^{N} \delta\rho(z_{i,i+1})\ \text{erfc}\left(\frac{z - z_i}{\sqrt{2}\sigma_i}\right), \tag{7}$$

where $\delta\rho(z_{i,i+1})$ is the density difference between two adjacent sublayers and σ_i is the root-mean-square roughness of interface i. We set the roughness of each artificial sublayer, except for the top one, to 0.0. Using this model, we obtain top roughness of 7–10 Å for $0° \leq \alpha \leq 60°$ and 20–30 Å for 80° samples. With increasing thickness of the thin film, the fitted top roughness increases. The thickness of the top layer is always chosen larger than its roughness. A roughness of 2–4 Å is obtained between the substrate and the porous film.

Assuming that the whole film consists only of Si (SiO_2 on columns is neglected), the porosity profile of a layer is approximated by

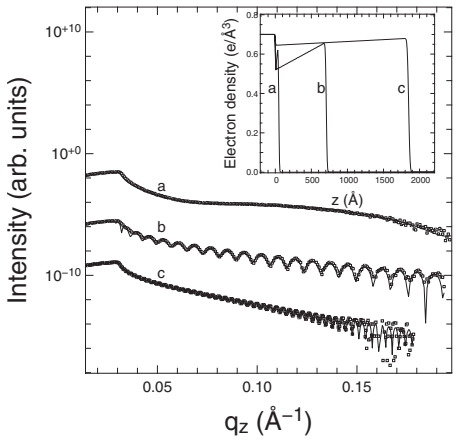

FIG. 5. Reflectivity curve (dots) and theoretical fits (solid line) of 0° GLAD sample of (a) 48, (b) 700, and (c) 1845 Å thicknesses. The curves are shifted on the intensity scale with respect to each other for clarity.

$$P(z) = 1 - \frac{\rho(z)}{\rho_{\mathrm{Si}}}. \tag{8}$$

Since electron densities of Si and SiO_2 are close (ρ_{Si} $=0.7\ e/\text{Å}^3$ and $\rho_{\mathrm{SiO_2}}=0.67\ e/\text{Å}^3$), this assumption will not cause any significant modification of our conclusions. The average density of the topmost layers determines the critical angle [Eq. (4)]. Due to the columnar porous structure of the films with increasing deposition angle, the critical angle (and average density of top layers) for each sample decreases.

C. Analysis of samples deposited with vapor incidence angle: $0° \leq \alpha \leq 60°$

Figure 5 depicts the reflectivity curves and theoretical fits of 0° samples on silicon substrate. For all samples, the critical angle of $q_z=0.03\ \text{Å}^{-1}$ corresponds to $0.7\ e/\text{Å}^3$ electron density on top. A linearly increasing density profile fits the data (insets of Fig. 5) and the porosity decreases from 8% in the bottom to 3% in the top layers. This positive slope gives the increasing oscillation amplitudes seen in the data.

The three density profiles for 0° samples (inset of Fig. 5) imply that as the films grow, the deeper parts of the films fill in. For the thinnest film, the precise density from the fit has a spatial variation which is beyond the resolution of the measured reflectivity. Using the increased intensity at a synchrotron would allow measurements to higher q and allow for a better determination of this density profile; however, one can believe that the initial formation of the thin film has a low average density and so is fairly porous or very rough. As the film grows, the density near the substrate increases with time. Fitting XRR data of 60° samples [Fig. 6(A)], the density profiles [Fig. 6(B)] reveal the similar behavior but with increased porosity, presumably due to shadowing.

D. Analysis of samples deposited with vapor incidence angle: $\alpha=70°$

Glancing-angle-deposited thin films with $\alpha>70°$ have been extensively studied in recent years.[12,14–16] Figure 7(A) depicts the reflectivity curves and their fits of 40°, 60°, and 70° samples in the 900–1050 Å thickness range. In these three samples, a linear density profile fits the data appropriately, but the slope of the 70° film changes, dramatically, to become negative [Fig. 7(B)]. Also, density profiles reveal that all the three samples have almost same densities up to 50 Å from the substrate, after which the density of 40° and 60° samples increase linearly and that of 70° sample falls to lower values. More physical conclusions can be inferred as follows:

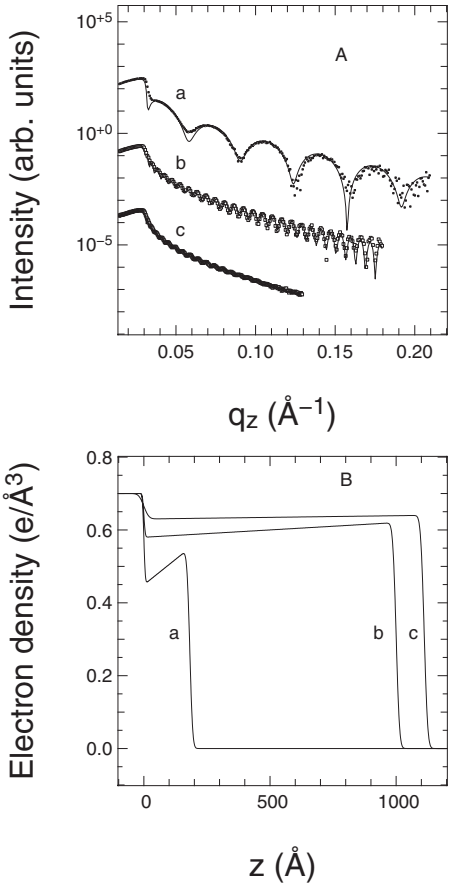

FIG. 6. (A) Reflectivity curve (dots) and theoretical fits (solid line) of 60° samples on silicon with (a) 180, (b) 1000, and (c) 1100 Å thicknesses. The curves are shifted on intensity axis with respect to each other for clarity. (B) Corresponding electron densities.

(i) In the very early stages of the growth, up to 50 Å from substrate, all samples show the same amount of porosity (about 10%). For the initial growth of the films, one would not expect shadowing to play a big role but to depend on how the particles accumulate on the substrate. The stochastic arrival of atoms during the first few atomic layers creates this nucleation layer, which can be considered to be very rough, or equivalently, quite porous.

(ii) After $z=50$ Å the shadowing effect intensifies for the 70° sample compared to the other two. In this thickness range, the influence of the shadowing over the film growth arranges columns diameter and their mutual separation to have a less dense film. Consequently, a more porous structure is created.

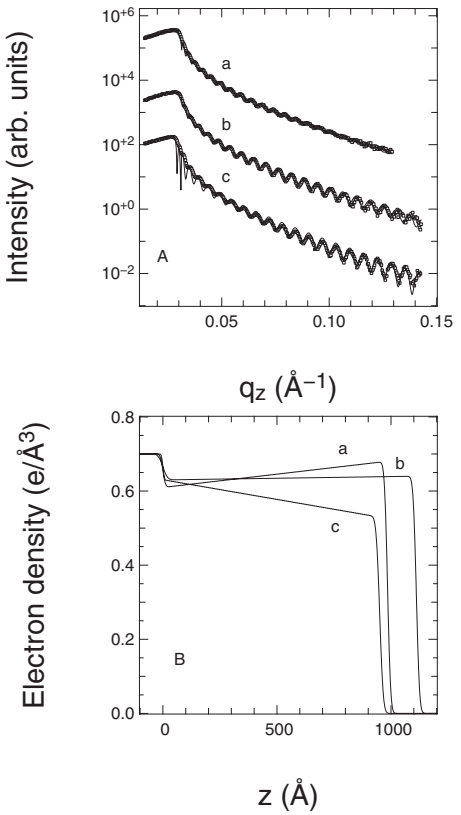

FIG. 7. (A) Reflectivity curve (dots) and theoretical fits (solid line) of (a) 40°, (b) 60°, and (c) 70° samples on silicon substrate. (B) Corresponding electron-density profiles.

In Fig. 8 the average porosity of the porous silicon samples with thickness of about 100 nm is graphed versus their deposition angle. It reveals that average film porosity increases slightly as the deposition angle is increased from 0° to 60° then increases dramatically for films deposited at 70° or higher (Tables I and II).

E. Analysis of samples deposited with vapor incidence angle: α=80°

Increasing the deposition angle increases the effect of shadowing. Figure 1(a) schematically depicts the thickness evolution of highly porous films made with glancing-angle

TABLE I. Results obtained for samples on silicon with $0° \leq \alpha \leq 60°$.

Angle of deposition (α)	Nominal thickness d (Å)	Calculated thickness d (Å)	Average porosity $\bar{P}$ (%)
0°	500	700 ± 1	13 ± 1
0°	2000	1845	8
40°	1000	975	11
60°	100	180	40
60°	800	1000	15
60°	1000	1100	12

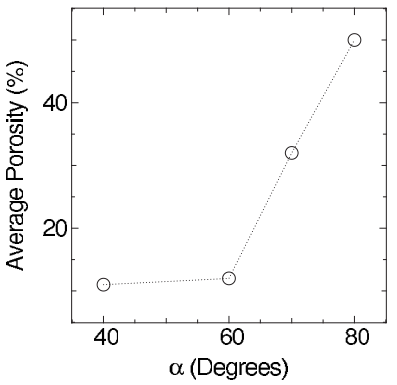

FIG. 8. The average porosity of GLAD samples with thickness of about 100 nm versus the deposition angle. The dashed line is a guide for the eyes.

deposition. This growth mode is essentially a competition for vapor flux, and columns are continually losing to their neighbors and becoming extinguished—they stop receiving flux due to shadowing and therefore stop growing. Figure 9 shows the reflectivity data and theoretical fit for 80° samples with various thicknesses on silicon substrate. For very thin layers, x rays are mostly reflected from substrate and the critical angle of the silicon substrate appears in the reflectivity curves. Thickness fringes with a large periodicity evidence the formation of a very thin layer of an average electron density different from the substrate [Figs. 9(a) and 9(b)].

In thicker samples ($d \geq 687$ Å), the appearance of a second critical angle smaller than the critical angle of silicon is a signature of lower density layer on top of the dense Si substrate. The falling density profile reproduces this feature. The position of the maxima between the two critical angles is described by Eq. (5).

A comparison of the three density profiles for thick samples ($d \geq 687$ Å) (inset of Fig. 9) reveals 25%–28% porosity for samples in the bottom layers up to 200 Å from the substrate, after which the porosity decreases faster for thicker samples. Table II summarizes the results for average porosity of the 70° and 80° samples and shows ≈50% average porosity (also, see Fig. 8).

F. Optical index of refraction

Using ellipsometry, measurements of the refractive index of GLAD samples have been reported.[16,24] The optical index of refraction decreases as the deposition angle grows to more

TABLE II. Results obtained from fitting for samples on silicon with $70° \leq \alpha \leq 80°$.

Angle of deposition (α)	Nominal thickness d (Å)	Calculated thickness d (Å)	Average porosity $\bar{P}$ (%)
70°	1000	941 ± 1	32 ± 1
80°	149	170	58
80°	746	880	49
80°	800	687	51
80°	1000	1030	50

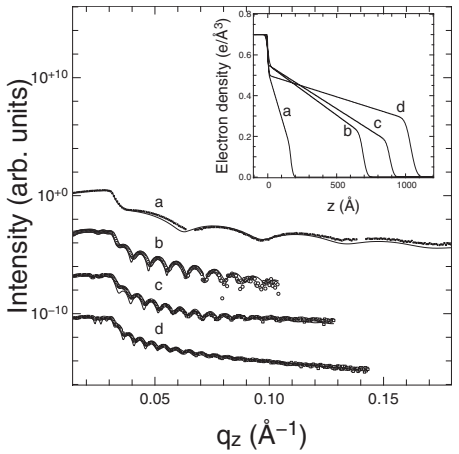

FIG. 9. Reflectivity curves and fits for 80° samples on silicon and corresponding EDPs in inset: (a) 170, (b) 687, (c) 880, and (d) 1030 Å. The curves are shifted on intensity axis for clarity.

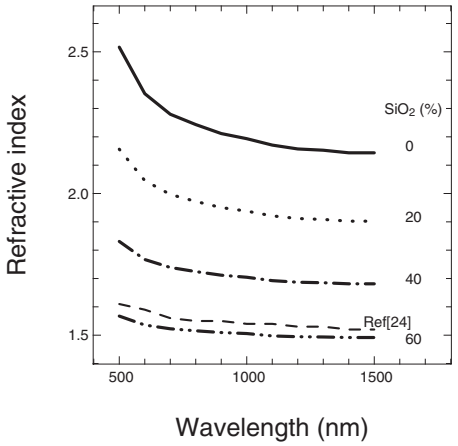

FIG. 10. Results of the EMA theory in calculating the index of refraction for 80° sample with 1000 Å nominal thickness. The index of refraction varies with the amount of SiO_2 and with wavelength. The calculated index of refraction in Ref. 24 is depicted.

than 70°. This was attributed to a porosity increase in the samples with higher deposition angles. Because of the large difference between the index of refraction of Si and SiO_2, the data could not be used to estimate the porosity. Having measured the porosity of our samples, we can estimate the amount of silicon oxide from the index of refraction data using the effective medium approximation (EMA).[25] EMA is used to evaluate the index of refraction of mixed component thin films. It assumes that subunits of the mixture are randomly mixed and that the subunit dimensions are much smaller than the incident wavelength. It makes sense to apply this approximation to our thin films.

In the EMA theory, the effective index of refraction of a medium is given by solving

$$\sum_i f_i \frac{n_i^2 - n_{\text{eff}}^2}{n_i^2 + 2n_{\text{eff}}^2} = 0, \tag{9}$$

where f_i and n_i are the volume fraction and refractive index of component i, respectively. Figure 10 shows the optical refractive indices of 80° sample of 1000 Å nominal thickness calculated by Eq. (9) for several assumed SiO_2 volume fractions. Comparing this data to the measurements in Ref. 24, we estimate slightly more than 50% volume fraction of SiO_2.

V. CONCLUSION

We used XRR technique to investigate porous GLAD samples and estimate their electron-density profiles versus depth. A simple linear model describes the density and porosity of the samples versus the depth of the films. Three main simple conclusions are demonstrated. First the density (or porosity) varies with depth. Second, at deposition angles between 60° and 70°, the films switch from having increasing density with thickness to decreasing density even though a constant deposition rate is used. Third, the density at a fixed height above the substrate increases with further deposition. These results place stringent constraints on any modeling of the growth processes. As well, calibration or modeling of these effects will be required to properly make GLAD films for graded index of refraction systems.

[1] L. T. Canham, Appl. Phys. Lett. **57**, 1046 (1990).
[2] W. H. Lowdermilk and D. Milam, Appl. Phys. Lett. **36**, 891 (1980).
[3] J. P. Zheng, K. L. Jiao, W. P. Shen, W. A. Anderson, and H. S. Kwok, Appl. Phys. Lett. **61**, 459 (1992).
[4] K. Robbie, G. Beydagian, T. Brown, C. Dean, J. Adams, and C. Buzea, Rev. Sci. Instrum. **75**, 1089 (2004).
[5] K. Robbie, D. J. Broer, and M. J. Brett, Nature (London) **399**, 764 (1999).
[6] S. R. Kennedy and M. J. Brett, Appl. Opt. **42**, 4573 (2003).
[7] G. S. Bales, R. Bruinsma, E. A. Eklund, R. P. U. Karnasiri, J. Rudnick, and A. Zangwill, Science **249**, 264 (1990).
[8] C. Roland and H. Guo, Phys. Rev. Lett. **66**, 2104 (1991).
[9] S. Lichter and J. Chen, Phys. Rev. Lett. **56**, 1396 (1986).
[10] A. Mazor, D. J. Srolovitz, P. S. Hagan, and B. G. Bukiet, Phys. Rev. Lett. **60**, 424 (1988).
[11] J. Krug and P. Meakin, Phys. Rev. A **43**, 900 (1991).
[12] K. Robbie, J. C. Sit, and M. J. Brett, J. Vac. Sci. Technol. B **16**, 1115 (1998).
[13] D. Vick, L. J. Friedrich, S. K. Dew, M. J. Brett, K. Robbie, M. Seto, and T. Smy, Thin Solid Films **339**, 88 (1999).
[14] K. Robbie, L. J. Friedrich, and S. K. Dew, J. Vac. Sci. Technol. A **13**, 1032 (1995).
[15] K. Robbie and M. J. Brett, J. Vac. Sci. Technol. A **15**, 1460 (1997).
[16] K. Kaminska, A. Amassian, L. Martinu, and K. Robbie, J. Appl. Phys. **97**, 013511 (2005).
[17] M. Tolan, *X-ray Scattering From Soft-Matter Thin Films*

(Springer, Berlin, 1999).
[18] J. Daillant and A. Gibaud, *X-ray and Neutron Reflectivity: Principles and Applications* (Springer, New York, 1999).
[19] J.-A. Nielson and D. McMorrow, *Elements of Modern X-ray Physics* (Wiley, New York, 2001).
[20] B. E. Warren, *X-ray Diffraction* (Dover, NewYork, 1990).
[21] A. Gibaud and G. Vignaud, Acta Crystallogr., Sect. A: Found. Crystallogr. **49**, 642 (1993).
[22] B. Vidal and P. Vincent, Appl. Opt. **23**, 1794 (1984).
[23] D. G. Stearns, J. Appl. Phys. **65**, 491 (1989).
[24] K. Kaminska, T. Brown, G. Beydaghyan, and K. Robbie, Appl. Opt. **42**, 4212 (2003).
[25] A. Feldman, Soc. Photo-Opt. Instrum. Eng. **821**, 129 (1987).